Analysis of Optical Emission towards Optimisation of Femtosecond Laser Processing

Y.Z. DENG[A], H. Y. ZHENG[B] *, V. M. MURUKESHAN[A], W. ZHOU[A]

[A] *School of MAE, Nanyang Technological University, Singapore*
[B] *Singapore Institute of Manufacturing Technology, Singapore*
71 Nanyang Drive, Singapore 638075
＊Corresponding author's Email: hyzheng@SIMTech.a-star.edu.sg

Abstract: Recent research and development on the femtosecond laser has shown that it is a powerful tool for high precision micromachining. However, femtosecond laser-material interaction is fast and complex due to its ultrashort pulse duration. As the laser-induced plasma possesses useful information to understand the physical mechanism of laser processing, we investigate the optical emission during femtosecond laser material processing. Laser-induced plasma spectra of brass, silicon and tin were captured using a fibre optic spectrometer. Key parameters of the plasma such as plasma temperature and electron density were estimated based on the spectral details. These results may serve as a necessary basis of further research into the development of on-line monitoring techniques for the optimisation of the femtosecond laser processing.

Keywords: optical emission, femtosecond laser processing, plasma spectra

1. Introduction

Femtosecond laser is a powerful tool for high precision micro-machining applications. It is particularly suitable for versatile applications such as drilling, cutting, fabrication of complex patterns and property modification [1, 2]. Compared to long-pulse laser sources, the ablation threshold is lowered and the energy deposited into the material is highly localised. Consequently, undesired thermal effects are greatly reduced and cleaner machined structures can be obtained [3].

Material removal with the femtosecond laser is a very fast and complex process. At femtosecond time scale, free electrons absorb laser energy and leave the sample surface in several picoseconds. Atoms and ions from the solid appear in nanosecond region. Meanwhile, dense plasma is formed above the surface of the sample [4, 5]. Currently, no generic model is available to describe the laser-matter-interaction dynamics. Signal diagnostics techniques can compensate for lack of mathematic models to optimise process parameters and ensure high-quality machining.

One powerful technique to investigate the physical mechanism of laser ablation is emission spectroscopy. Fundamental plasma parameters such as the electron temperature (T_e) and electron number density (n_e) can be obtained from optical emission spectra. Diagnostics of nanosecond laser- induced plasma have been widely reported [6 - 10]. Femtosecond laser-induced plasma is currently being investigated [4, 11, 12]. In this paper, we study the plasma emission during femtosecond laser processing, which contains significant information about the nature of the process.

The spectroscopic analysis of the femtosecond laser-induced plasma was conducted for different materials. Key parameters such as plasma temperature and electron density were estimated. They help in describing the femtosecond laser-material interaction mechanism. This work provides improved understanding for further research to develop on-line monitoring system for femtosecond laser material processing.

2. Experimental set-up

The schematic diagram of the experimental set-up is presented in Fig. 1. The output laser beam from the amplified Ti:Sapphire laser system (Clark-MXR CPA-2001) was directed to the sample by the beam delivery system. It was focused onto the sample surface using a plano-convex quartz lens with a focal length of 50 mm. The focusing lens is fixed on a linear stage, which moves up and down. The sample is placed on a 2-axis translation stage for movement in both x and y directions. All the stages are controlled by the computer. The optical emission of the plasma was collected by a UV/VIS spectrometer (Ocean Optics USB2000) through a multimode fibre. The spectra range of the spectrometer is 200-850 nm with a resolution of 1.33 nm. The detector of the spectrometer is a Sony ILX511 linear CCD array, which has 2048 pixels with a pixel size of 14 μm × 200 μm.

The femtosecond laser used in the experiments has a wavelength of 775 nm and the pulse duration of 150 fs. It is a fully integrated Ti:Sapphire laser system based on the chirped pulse amplification technique. The seed-laser is generated by the fiber ring oscillator, which uses erbium doped fiber as the gain medium. It is pumped by an all solid-state fiber-coupled laser diode operating at approximately 980nm. The amplification of the seed-laser is achieved by the pulse stretcher, the regenerative amplifier pumped by the Nd:YAG laser and the pulse compressor. After amplification, the pulse energy is increased to 0.8 mJ at a repetition rate of 1kHz.

3. Results

To investigate the optical emission during the femtosecond laser ablation, the laser-induced plasma of different materials, such as brass, silicon and tin, was captured by the optical spectrometer. As time-integrated spectra were used to estimate plasma parameters, T_e and n_e in the following paragraphs refer to time-averaged values of electron temperature and electron density. They are approximations of the time-varying electron temperature and electron density.
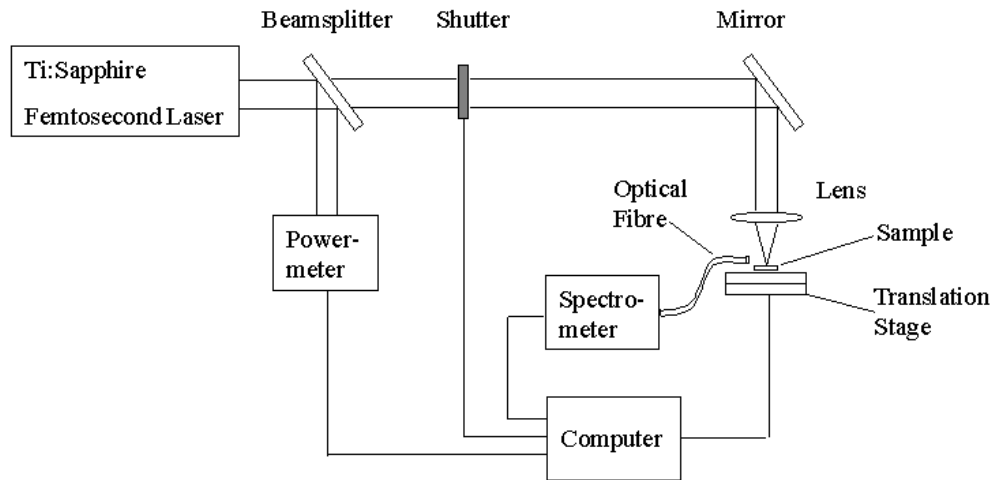
Fig. 1 Schematic diagram of the experimental setup

3.1 Time-averaged electron temperature of the brass sample

The time-integrated spectrum of the brass sample under laser power of 264 mW is presented in Fig. 2. The emission lines for Cu I were observed at 405.6 nm, 427.2 nm, 447.5 nm, 458.5 nm, 510.2 nm, 515.1 nm, 521.3 nm, 569.5 nm and 577.7 nm, while the emission lines for Zn I were observed at 471.9 nm, 480.7 nm and 636.3 nm. These emission lines were mainly located in the visible light range. Compared to the emission lines listed in the standard database [13, 14], it is observed that there are differences approximately less than 1 nm, which can be attributed to the limited resolution of the spectrometer and phase-shift during laser ablation. The spectroscopic parameters are presented in Table 1 [13 - 15]. It is shown that the observed emission lines are of different types of transitions [16] and their upper energy levels distribute in the range of 3.8 eV to 7.8 eV.

Compared to the time-resolved spectra of copper targets in air [16], only neutral atom lines were detected in our time-integrated spectra of brass sample. Those short-lifetime emission lines, such as Cu ionic lines and lines from air components (nitrogen and oxygen) were not observed in our study. To capture those emission lines, suitable gating time and a delay time shorter than 200 ns were used [16].

Under the assumption of local thermodynamic equilibrium (LTE), the plasma temperature can be estimated using relative intensities of the emission lines from the same atomic or ionic species [6, 7, 11]. If the level populations are distributed according to the Boltzmann law, the relative intensity of the emission line is described by

$$\ln\left(\frac{\lambda I}{A_{ki} g_k}\right) = C - \frac{E_k}{kT_e} \qquad (1)$$

where I, λ, A_{ki}, g_k, E_k, k and T_e are the relative intensity, wavelength, the transition probability, the statistic weight of the upper level, the energy of the upper level, Boltzmann's

constant and electron temperature. With the measured relative intensities of several spectral lines, a plot of the logarithmic term in Eqn. (1), versus E_k can be plotted. It is a straight line with a slope equal to $-1/kT_e$. Based on this linear equation, T_e can be obtained readily.

Table 1 Spectroscopic data of emission lines detected in the plasma of the brass sample

Wave-length λ (nm)	Upper energy level E_k (eV)	Lower energy level E_i (eV)	Transition probability A_{ki} (10^8 1/s)	Statistical weight of the upper level g_k
Cu (I) 406.3	6.9	3.8	0.21	6
Cu (I) 427.5	7.7	4.8	0.35	8
Cu (I) 448.0	6.6	3.8	0.03	2
Cu (I) 458.7	7.8	5.1	0.32	6
Cu (I) 510.6	3.8	1.9	0.02	4
Cu (I) 515.3	6.2	3.8	0.60	4
Cu (I) 521.8	6.2	3.8	0.75	6
Cu (I) 570.0	3.8	1.6	2.5×10^{-3}	4
Cu (I) 578.2	3.8	1.6	0.017	2
Zn (I) 472.2	6.7	4.0	-	-
Zn (I) 481.1	6.7	4.0	-	-
Zn (I) 636.2	7.7	5.8	0.474	5

Following Eqn. (1), the Boltzmann plot for emission lines in Fig. 2 is shown in Fig. 3. The linear equation of the fitting line in this figure is given by

$$\ln\{\lambda I/(A_{ki}g_k)\} = -1.4E_k + 23.6 \qquad (2)$$

Consequently, T_e is calculated to be 8293.8 K. For accurate estimation of the electron temperature using the Boltzmann

plot method, the ideal emission lines should be in close spectral proximity, with reasonable intensity, of known transition probability and with different upper energy levels [17]. However, it is difficult to find enough emission lines meeting all these requirements, especially for time-integrated spectra obtained by non-gated detection. Usually, the main errors associated with the Boltzmann plot are inaccuracy of the transition probability and limited range of the upper energy level [11, 18]. In our case, overlapping of the emission lines also increased the estimation error, although three-peak Lorentzian fitting was used to calculate the emission line intensity.

When estimating the electron temperature using the Boltzmann plot method, it is assumed that the plasma is in the LTE condition, i.e. atomic and ionic states should be populated and depopulated predominantly by collisions rather than by radiation. The lower limit of the electron density n_e to ensure a high collision rate is given by [8, 11]

$$n_e\left(cm^{-3}\right) \geq 1.4 \times 10^{14} T_e^{1/2} \Delta E^3 \tag{3}$$

where ΔE (in eV) is the energy difference between the upper and lower states, and T (in eV) is the plasma temperature.
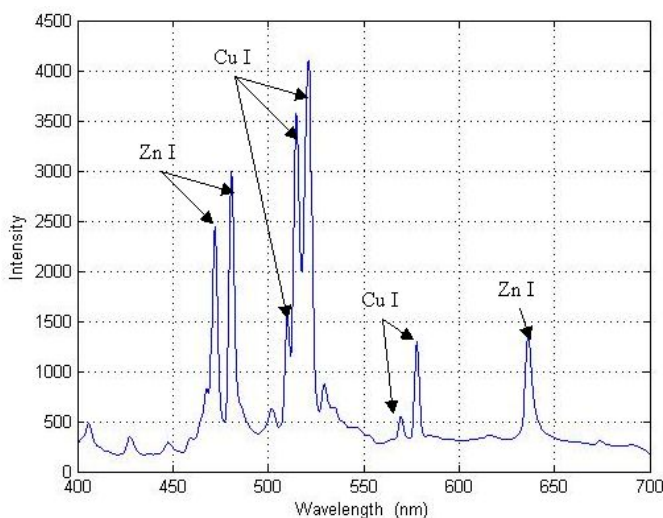
Fig. 2 Time-integrated spectra of a brass sample
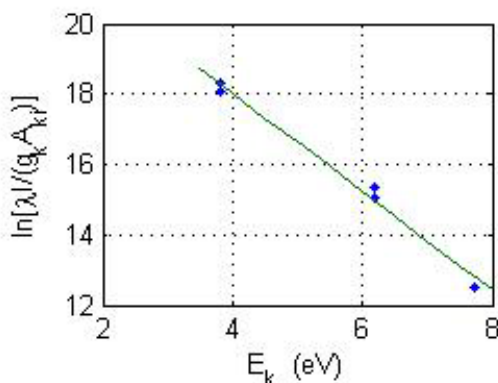
Fig. 3 Boltzmann plot for temperature estimation of a brass sample

To verify the LTE assumption using Eqn. (3), the electron density n_e is required. The method to estimate n_e using the emission line will be discussed in next section. However, we do not have the required parameter of copper to estimate n_e. Alternatively, the emission lines of Zn (I) were used to calculate n_e. The spectroscopic data for Zn were obtained from [14, 19]. A similar analysis was reported in [20], in which the N II 399.5 nm line was used to estimate the electron density because the authors were short of data of copper. It is said that the emission line of N II 399.5 nm only appeared in the early 300 ns. In our study, this short lifetime emission line was not observed. For $kT_e < 1$ eV and $\Delta E < 3.5$ eV, the lower limit of n_e given in Eqn. (3) is about 6×10^{15} cm^{-1}. As the estimated n_e in our case is 5×10^{17} cm^{-1}, higher than the lower limit of n_e, the necessary condition for LTE is satisfied.
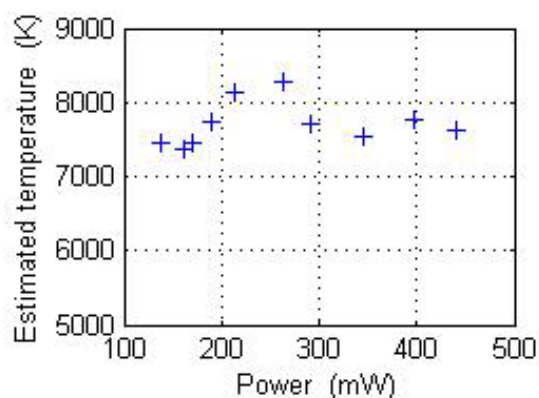
Fig. 4 Estimated plasma temperature of a brass sample under different laser power

The time-averaged electron temperature T_e under different incident laser power is shown in Fig. 4. When the laser power varied from 137 mW to 440 mW (corresponding to the intensity level of ~ 1 TW / cm^2 when the spot diameter on the sample is about 0.05 mm), T_e changed in the range of 7355 K to 8294 K. The temperature reached its peak at 264 mW and decreased to a lower level at higher laser power. The variation of T_e is smaller than 14 %. In our study, T_e is estimated using time-integrated emission spectra, which is also integrated along the line-of-sight. Therefore, it is a time- and space- averaged value. It is difficult to draw a conclusion on the dependence of the electron temperature on the laser power using this averaged value because electron temperature is time- and space- dependent [6, 8, 11]. T_e decreases as the plasma cools down and T_e in the center of the plasma is higher than that at the outer space [11, 18]. As T_e in Figs. 3 - 4 was estimated using Cu I emission lines, it may be considered as an indication of the electron temperature in the outer region of the plasma because there are more neutral atoms than ions in this region. On the contrary, we are not able to estimate the higher electron temperature at the plasma center since almost no neutral emission is produced at this region [18]. Other factors that may influence our results include the interaction of laser pulses with the ambient gas: air [21], and the mechanism of plasma absorption of femtosecond laser pulses [22]. To further clarify this issue, temporal and spatial character-

istics of the plasma should be investigated by adoption of gated detection and a deconvolution process, such as the Abel inversion [18]. Moreover, inert gas should be used as the ambient gas for comparison.

3.2 Time-averaged electron temperature and electron density of the silicon sample

Another example is the time-integrated spectra of the silicon sample under different laser power as shown in Fig. 5. The emission lines detected were Si I 243.9 nm, 252.1 nm, 263.3 nm, 288.5 nm, 298.8 nm and 390.1 nm. In addition, emission lines for Si II were also observed at 385.4 nm and 412.5 nm. The spectroscopic data of these emission lines are presented in Table 2 [8, 14]. There were small errors in wavelength due to spectrometer resolution and phase-shift as mentioned in section 3.1. As the power of the laser pulse increased, both the magnitudes of the emission lines and continuum emission increased. The continuum is related to the collisions between the free electrons and the excited atoms and ions, and the recombination of electrons with ions. Different from the spectra of nanosecond laser-induced plasma in [8], strong continuum emission at the initial stage of plasma generation was not observed. The femtosecond laser-induced plasma cools quickly and the plasma lifetime is shorter than that of the nanosecond laser-induced plasma [11, 12].
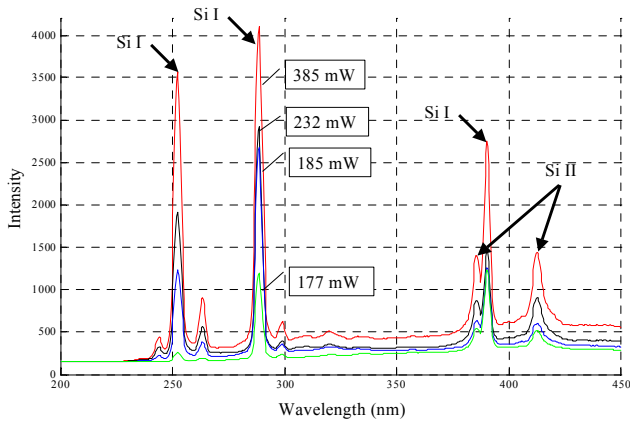
Fig. 5 Time-integrated spectra of a silicon sample

It is shown in section 3.1 that the electron temperature T_e can be estimated using the Boltzmann plot under the LTE condition. However, for the emission lines of Si (I) in Fig. 5, the energy spread is quite limited, less than 2 eV. Therefore, it is difficult to estimate the excitation temperature accurately using the Boltzmann plot. A modified approach is to combine the Saha equation with the Boltzmann equation. By adopting both emission lines of atoms and ions, a wider range of the upper level energies is obtained, thus increasing the accuracy of temperature estimation [18, 22]. The modified equation is

$$\ln\left(\frac{\lambda I}{A_{ki} g_k}\right)^* = C - \frac{E^*}{kT_e} \tag{4}$$

Table 2 Spectroscopic data of emission lines detected in the plasma of the silicon sample

Wavelength λ (nm)	Upper energy level E_k (eV)	Lower energy level E_i (eV)	Transition probability A_{ki} (10^8 1/s)	Upper statistical weight g_k
Si (I) 243.9	5.1	0	7×10^{-3}	3
Si (I) 252.4	4.9	9.6×10^{-3}	1.81	1
Si (I) 263.1	6.6	1.9	0.97	3
Si (I) 288.2	5.0	0.8	1.89	3
Si (I) 298.8	4.9	0.8	2.2×10^{-2}	3
Si (I) 390.6	5.1	1.9	0.118	3
Si (II) 385.4	10.1	6.7	0.25	2
Si (II) 412.8	12.8	9.8	1.32	6

In Eqn. (4), the abscissa value of the ion energy level, E^*, is obtained by adding a corrected ionisation potential to the ion energy level:

$$E^* = E_k + E_{IP} - \Delta E \tag{5}$$

where E_{IP} is the ionisation potential of the less ionised stage and ΔE is a correction to the ionisation potential for interactions in the plasma [18, 22]. The ion ordinate value is obtained by subtracting an entropy-related term [18, 22],

$$\ln\left(\frac{\lambda I}{A_{ki} g_k}\right)^* = \ln\left(\frac{\lambda I}{A_{ki} g_k}\right) - \ln\left\{\frac{2(2\pi m_e k)^{3/2}}{h^3} \frac{1}{n_e} T_e^{3/2}\right\} \tag{6}$$

where m_e is the rest mass of the electron and h is Plank's constant. For neutral atoms, the corrections in Eqns. (5) and (6) have no effect.

As the correction term in Eqn. (6) depends on the unknown parameter T_e, it will be determined by an iterative approach [18, 22]. First, the ordinates of the ions are calculated using an initial guess of the temperature; then a new temperature is determined from a linear fit of the Saha-Boltzmann plot for both neutral atoms and ions. This new temperature is used to adjust the ion ordinates for next linear fitting. This iterative procedure is repeated until the temperature value converges. This approach is feasible because $1/T_e$ in Eqn. (4) varies much more rapidly than $\ln(T^{3/2})$. The correction term in Eqn. (6) also depends on the electron density n_e, but the Saha-Boltzmann plot is not very sensitive to changes in n_e. Usually, n_e is estimated from measurement of the Stark broadening of the emission lines.

By Lorentzian fitting of the Stark-broadened line profile of an isolated atom, the line width (FWHM) can be obtained that is related to the electron density n_e by the following expression [6 - 8],

$$\Delta\lambda_{1/2} = 2W\left(\frac{n_e}{10^{16}}\right) + 3.5A\left(\frac{n_e}{10^{16}}\right)^{1/4}\left(1 - 0.75N_D^{-1/3}\right)W\left(\frac{n_e}{10^{16}}\right) \tag{7}$$

In Eqn. (7), $\Delta\lambda_{1/2}$ is in nm and electron number density n_e is in cm^{-3}. The coefficients W and A are the electron impact-width parameter and the ion-broadening parameter, which are weak functions of temperature [8]. N_D is the number of particles in the Debye sphere. In Eqn. (7), the first term is related to the electron broadening and the second term is related to the ion-broadening correction. As the

second term is typically very small and negligible, Eqn. (7) can be reduced to

$$\Delta\lambda_{1/2} = 2W\left(\frac{n_e}{10^{16}}\right) \tag{8}$$

Based on the emission line at 288.2 nm in Fig. 5, the time-integrated electron density of silicon under a laser power of 385 mW is estimated to be 1.8×10^{19} cm^{-3}.

The Saha-Boltzmann plot using the emission lines of the spectrum of the silicon sample is shown in Fig. 6. Now the energy range is increased to 16 eV by adding the data of the ions. Under the laser power of 385 mW (corresponding to an intensity of ~1.3 TW / cm^2), the estimated temperature is 21616K. For kT < 2 eV and ΔE < 5.1 eV, the lower limit for n_e is 2.7 x 10^{16} cm^{-1}, which is much lower than the estimated value of n_e. Therefore, the assumption of LTE is valid. The estimated T_e is a time- and space- averaged value of the electron temperature, which is influenced by several factors, including uncertainty of the transition probability, overlapping of emission lines and selection of the emission lines for calculation.
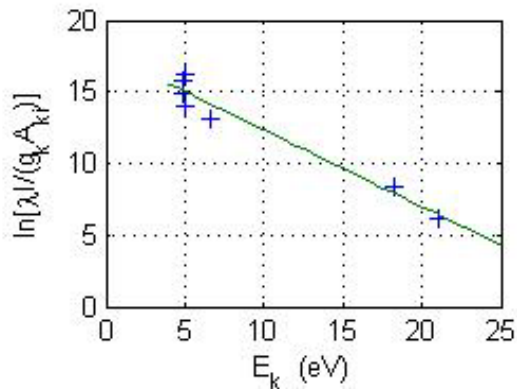
Fig. 6 Saha-Boltzmann plot for temperature estimation of a silicon sample
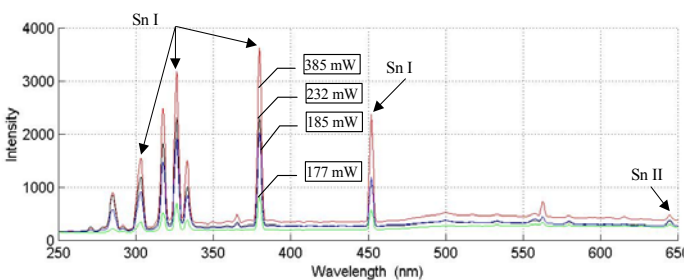
Fig. 7 Time-integrated spectra of a tin sample

3.3 Plasma spectroscopy of the tin sample

The third example is the time-integrated spectra of the tin sample under different laser power as shown in Fig. 7. The emission lines for Sn I were observed at 285.0 nm, 303.0 nm, 317.6 nm, 326.1 nm, 333.0 nm, 365.1 nm, 379.6 nm, 452.1 nm and 562.7 nm. Moreover, the emission line for Sn II at 644.6 nm was also detected. The magnitudes of these emission lines are larger at a higher incident laser power. As we do not have enough spectroscopic data of these emission lines, we are not able to estimate the electron temperature and density of the plasma.

4. Conclusions and discussions

Plasma temperature and profile are closely related to thermal-related quality issues such as heat-affected-zone and thermal-induced cracks when processing brittle materials as plasma is a hot source. Plasma can also be related to material re-depositions as the ablated materials fall back onto substrate surfaces. Plasma analysis will help understand its profile, composition and intensity, which has significant influence on the quality issues.

The time-integrated spectra of the femtosecond laser-induced plasma of different materials are presented in this paper. During the experiments, the whole emission transient was captured by the spectrometer and the results obtained were approximations of the very fast dynamics of the plasma. To investigate the time-varying functions of the plasma profile and parameters, a high-speed gating device should be adopted and the gate width of the boxcar should be set much smaller than the transient time of the plasma. In addition, a high sensitivity detector such as ICCD or PMT is required to capture very weak optical signals. Although such equipment is indispensable for academic research, it is too complicated and expensive for industrial applications.

Although non-gated detection was used in our study, the continuum observed was much smaller than emission spectral lines of interests and a good signal-to-noise ratio was obtained. It is the result of significant reduction of the continuum emission in the early phase of the formation of femtosecond laser-induced plasma [11, 12]. Low cost and ease of implementation associated with the time-integrated spectrum enable it to be used as a diagnostics tool for on-line monitoring of the femtosecond laser-material processing.

Currently, more work is in progress to study the relationship between the time-integrated plasma characteristics and time-resolved plasma characteristics. This will provide useful information to compensate for the limitation of time-integrated spectra and helps in developing practical on-line monitoring techniques for the femtosecond laser material processing.

References

[1]   D. Buerle™: "Laser Processing and Chemistry", 3rd Ed. Springer-Verlag Berlin Heidelberg (2000)

[2]   Craig, Laser Focus World, **34**, 79 (1998)

[3]   V. Hertel, R. Stoian, D. Ashkenasi, A. Rosenfeld and E. E. B. Campbell: Riken Review, **32**, 23 (2001)

[4]   V. Margetic, A. Pakulev, A. Stockhaus, M. Bolshov, K. Niemax and R. HergenrÖder: "Spectrochimica Acta Part B", 55, 1771 (2000)

[5]   Lawrence Berkeley National Laboratory website, http://tdhplc.lbl.gov/index.htm

[6]   Y. F. Lu, Z. B. Tao and M. H. Hong: Jpn. J. Appl. Phys., **38**, 2958 (1999)

[7]   M. J. Ying, Y. Y. Xia, and Y. M. Sun: Laser and Particle Beams, **21**, 97 (2003)

[8]   H. C. Liu, X. L. Mao, J. H. Yoo and R. E. Russo: "Spectrochimca Acta Part B", 54, 1607 (1999)

[9]   El-Astal, S. Ikram, and T. Morrow: J. Appl. Phys., **77**, 6572 (1995)

[10]   S. S. Harilal, C. V. Bindhu, and Riju C. Issac: J. Appl. Phys., **82**, 2140 (1997)

[11]   Le Drogoff, J. Margot, and M. Chakera: "Spectro chimica Acta Part B", 56, 987 (2001)

[12]   X. Zeng, X. Mao, and R. Greif: Appl. Phys. A, **80**, 237 (2005)

[13]   CRC Handbook of Chemistry and Physics, Cleve land: CRC Press.

[14]   NIST Atomic Spectra Database, http://physics.nist.gov/cgi-bin/AtData/display.ksh

[15]   Kurucz Atomic Line Database, http://cfa-www.harvard.edu/amdata/ampdata/amdata.html

[16]   B. Német and L. Kozma: "Spectrochimica Acta Part B", 50, 1869 (1995)

[17]   M. Milan, J. J. Laserna: "Spectrochimica Acta Part B", 56, 275 (2001)

[18]   J. A. Aguilera, C. Aragón: "Spectrochimica Acta Part B", 59 1861 (2004)

[19]   M. S. Dimitrijević and S. Sahal-Bréchot: Astron. Astrophys. Suppl. Ser., **140**, 193 (1999)

[20]   B. Y. Man, Q. L. Dong, and A. H. Liu: J. Opt. A: Pure Appl. Opt. **6**, 17 (2004)

[21]   J. Sun and J. P. Longtin: J. Appl. Phy, **89**, 8219 (2001)

[22]   H. Fan, J. Sun and J. P. Longtin: Journal of Heat Transfer , **124**, 275 (2002)

[23]   Yalcin, D. R. Crosley, G. P. Smith and G.W. Faris: Appl. Phys. B , **68**, 121 (1999)

[24]   H. R. Griem: "Plasma Spectroscopy", McGrawHill, New York (1964)